Journal of Power Sources 284 (2015) 16–26

Contents lists available at ScienceDirect

Journal of Power Sources

journal homepage: www.elsevier.com/locate/jpowsour

Study of CO_2 recovery in a carbonate fuel cell tri-generation plant

Giorgio Rinaldi [a, b], Dustin McLarty [a], Jack Brouwer [a, *], Andrea Lanzini [b], Massimo Santarelli [b]

[a] National Fuel Cell Research Center, University of California, Irvine, CA 92697, USA
[b] Department of Energy, Politecnico di Torino, C.so Duca degli Abruzzi 24, 10129 Torino, Italy

HIGHLIGHTS

- Separation of CO_2 in a biogas plant that co-produces electricity, hydrogen, and heat.
- The ability of MCFC is to concentrate CO_2 in the anode exhaust stream.
- Three cathode inlet configurations are considered.
- Results illustrate a high compatibility between hydrogen co-production and CO_2 recovery.
- A series configuration of MCFC technology coupled with an ICE achieves outstanding carbon recovery (exceeding 90%).

ARTICLE INFO

Article history:
Received 16 September 2014
Received in revised form
4 February 2015
Accepted 26 February 2015
Available online 27 February 2015

Keywords:
Tri-generation plant
Molten carbonate fuel cell
CO_2 separation
Hydrogen

ABSTRACT

The possibility of separating and recovering CO_2 in a biogas plant that co-produces electricity, hydrogen, and heat is investigated. Exploiting the ability of a molten carbonate fuel cell (MCFC) to concentrate CO_2 in the anode exhaust stream reduces the energy consumption and complexity of CO_2 separation techniques that would otherwise be required to remove dilute CO_2 from combustion exhaust streams. Three potential CO_2 concentrating configurations are numerically simulated to evaluate potential CO_2 recovery rates: 1) anode oxidation and partial CO_2 recirculation, 2) integration with exhaust from an internal combustion engine, and 3) series connection of molten carbonate cathodes initially fed with internal combustion engine (ICE) exhaust. Physical models have been calibrated with data acquired from an operating MCFC tri-generating plant. Results illustrate a high compatibility between hydrogen co-production and CO_2 recovery with series connection of molten carbonate systems offering the best results for efficient CO_2 recovery. In this case the carbon capture ratio (CCR) exceeds 73% for two systems in series and 90% for 3 MCFC in series. This remarkably high carbon recovery is possible with 1.4 MWe delivered by the ICE system and 0.9 MWe and about 350 kg day^{-1} of H_2 delivered by the three MCFC.

1. Introduction

The global impacts of CO_2 emissions from power generation have been well established [1]. Industrialized nations have made strong commitments for the reduction of CO_2 and other greenhouse gas emissions [2]. This presents a considerable technical challenge and significant driver for change to the power industry. Leading solutions include the introduction of large amounts of renewable power, more efficient systems for electricity production, more efficient transmission and use of electricity, and carbon capture and sequestration from fossil fuel plants. Most projections for future power generation include substantial contributions from fossil fuel combustion [3] to complement the cost, control and intermittency features of renewable power generation. Carbon separation in traditional fossil fuel power plants can be achieved either upstream or downstream of the combustion zone using a variety of technologies including cryogenics, air separation, and oxy-combustion [4], [5], [6]. Moreover, in recent years the opportunities for CO_2 recovery have grown considerably. Pure captured CO_2 is indeed a potential valuable feedstock for the synthesis of chemicals and synthetic fuels. Utilization rather than geological sequestration is also related to the poly-generation approach, i.e., energy systems featuring the co-production of several products (heat, electric power and chemicals).

* Corresponding author.
E-mail address: jbrouwer@uci.edu (J. Brouwer).

http://dx.doi.org/10.1016/j.jpowsour.2015.02.147
0378-7753/

Nomenclature

ASU	Air separation unit
α	charge transfer coefficient
CCR	Carbon capture ratio
CCS	Carbon capture and separation
CHP	Combined heat and power
F	Faraday constant [96485 C mol^{-1}]
HSU	Hydrogen separation unit
I	Current [A]
ICE	Internal combustion engine
LHV_{CH4}	Biogas lower heating value [800 MJ $kmol^{-1}$]
MCFC	Molten carbonate fuel cell
NFCRC	National Fuel Cell Research Center
$\dot{N}_i$	Molar flow of the species "*i*" [kmol s^{-1}]
η	Electrical efficiency
OCSD	Orange County Sanitation District
P_{el}	Electric power [kW]
$P_{el,\ ICE}$	ICE equivalent electric power [kW]
PSA	Pressure swing adsorption
STC	Steam to carbon ratio
T	Temperature
U_f	Fuel utilization factor
U_{CO2}	CO_2 utilization factor
V	Voltage [V]
WGS	Water gas shift
X_i	Molar concentration of the species "*i*"
y_{CH4}	Biogas composition – methane molar concentration

In this paper, a poly-generation system based on molten carbonate fuel cell is first studied, and new structures of the system are analyzed in order to provide a carbon recovery added effect. The transportation sector is searching for alternatives to traditional liquid hydrocarbon fuels by considering electricity, natural gas, biofuels and hydrogen, amongst other alternative fuels. Co-production of electricity and hydrogen with a molten carbonate fuel cell presents a unique opportunity for synergistic co-production with efficient carbon capture. High temperature fuel cells, especially molten carbonate (MCFC) and solid oxide fuel cells (SOFC), have received substantial attention during the past decades and have recently begun to achieve commercial success [7], [8]. Both MCFC and SOFC technologies can operate on natural gas and biogas to achieve higher fuel-to-electric (FTE) efficiencies and near zero criteria pollutant emissions (e.g. NOx, SOx, particulate) compared to traditional engines. Efficiency is further increased through the concept of "tri-generation", in which electrical power, thermal power and hydrogen are co-produced from a single fuel stream [9]. Tri-generation utilizes waste heat and chemical recovery concepts to produce a viable fuel that can be used for zero emission transportation purposes, as promoted by the state of California since the year 1990 [10]. With natural gas as a feedstock, CO_2 emissions can be lowered between 10 and 43.6% with a high temperature fuel cell, depending upon the electric power generating system considered in the comparison, while with renewable biogas feedstock the emissions can be reduced near to zero [11].

With this in mind, the current work investigates a further reduction of greenhouse gas emissions adding the recovery of CO_2 from a tri-generation MCFC plant. The energy intensity of CO_2 recovery is reduced when exploiting the carbonate ion transfer mechanism of molten carbonate fuel cells (Fig. 1). MCFC consume CO_2 in the cathode compartment and produce CO_2 in the anode compartment where it is only mixed with a small amount of fuel and product constituents (e.g., H_2, CO, water). When this anode exhaust stream is fully converted the CO_2 is only mixed with water allowing simple and inexpensive pure CO_2 recovery by cooling and water condensation.

Subsequent to the anode the remaining hydrogen content of the anode exhaust stream is typically oxidized in a combustor. To eliminate the introduction of nitrogen and excess oxygen the current design utilizes nearly stoichiometric oxy-combustion with oxygen supplied from an air separation unit. The resulting products of combustion, H_2O and CO_2, are readily separated with considerably less energy input than cryogenic CO_2 distillation. The plant configurations outlined in section 5 are an extension of the existing MCFC tri-generation plant located at the Orange County Sanitation District [12]. A molten carbonate fuel cell is fed with biogas produced on-site from the anaerobic digestion of sludge available in the wastewater treatment plant. This study outlines the feasibility of applying carbon sequestration to an already existing and operating MCFC tri-generation plant, with the aim of exploring synergies and limitations arising from the integration of a CO_2 recovery unit in a tri-generation plant co-producing electrical power, heat and hydrogen.

The CO_2 recovered could be recycled since its purity is sufficiently high. For example it could be sold as a commercial product in the food or chemical industry. Another possible use is the reconversion to fuel (e.g., in a photo-bio-reactor with the aid of nutrients (phosphates and nitrates) the added CO_2 stream can be converted to algae and oxygen). A third option is the transportation in pipeline to suitable sites for CO_2 sequestration. At present, a large share of CCS occurs through the injection in geological deposits previously used for the extraction of oil or gas. The combination of these techniques with a tri-generation system operated on biogas (such as the one at OCSD) would enable carbon-negative production of electricity and fuel (with the CCS process), since the carbon of the ADG was previously contained in the sewage (before being converted into biogas), which ultimately comes from plants that removed CO_2 from the atmosphere.

2. Background

Molten carbonate fuel cells utilize carbonate ions as the charge carriers in the electrochemical conversion of chemical energy into electrical energy. Operation between 550 and 650 °C is necessary in order to maintain a sufficient electrolyte conductivity and chemical reactivity without the use of noble metal catalysts. The

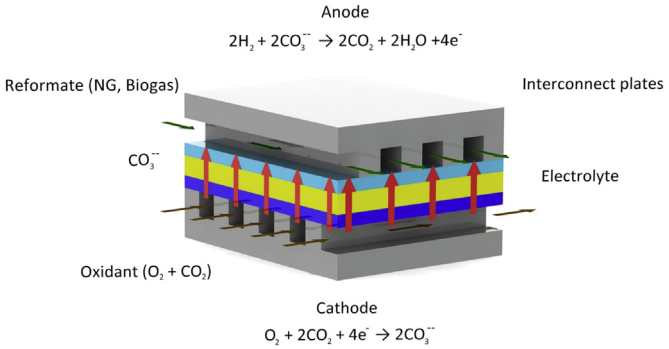

Fig. 1. Molten carbonate fuel cell.

temperature is well-suited for integration with hydrocarbon reformation in a fuel processor. The typically endothermic reactions which convert common fuels such as methane, biogas or ethanol into a hydrogen-rich feedstock is able to provide a substantial portion of the stack cooling requirement. The reformation process can occur directly within the anode gas channels and/or in separate in-stack plate reformers, as is the case for the current MCFC system.

Use of a MCFC as a carbon dioxide concentrator was investigated experimentally by Sugiura et al. [13], where it is showed that the experimental values for the CO_2 removal rate from cathode to anode performed in a MCFC almost matched theoretical calculations. One key conclusion from this work is that the ratio between the partial pressures of oxygen and carbon dioxide directly affects the performance. Campanari et al. [14] investigated the possibility of separating CO_2 from NG-fed combined cycles integrated with MCFC operating in the exhaust. Results identified the potential for an 80% reduction in CO_2 with negligible impact on electrical efficiency. This reduction was achieved with a MCFC sized to contribute only 20% of the net power generation. A similar study considered cryogenic separation of CO_2 from combined cycles integrated with MCFC [15] by analyzing the possibility of recirculating a portion of the carbon dioxide recovered in the cathode, thereby controlling the utilization of CO_2. This approach avoided the separation via oxy-fuel combustion presented in Campanari et al.

A subsequent paper from the same research group [16] compared three configurations for integrating a MCFC with an internal combustion engine. Carbon emissions from the combined system are dramatically reduced. Separate research has demonstrated this type of plant is, at the moment, un-profitable, but future cost reductions and incentives for fuel cells and avoided carbon emissions make this an attractive technology [17]. The economic analysis considered a small MCFC integrated with a CHP plant capable of separating 63% of the inlet carbon quantity at an overall fuel-to-electric efficiency of 35%. Further improvements in performance may improve the viability of MCFC CO_2 capture as much as potential cost reduction.

3. Model description

3.1. General overview on the model

The integration of a MCFC, hydrogen separation and CO_2 separation results in a highly coupled system requiring simulation with detailed physical models of the various sub-systems. This work extends the spatially resolved MCFC system modeling capability of the NFCRC and is comprised of multiple physical models of subsystem components that can be found in the literature [18], [19], [20].

The primary component model is that of the MCFC stack which has been designed and calibrated to represent the physics of the “FuelCell Energy Direct Fuel Cell” (DFC) design. The model permits variable flow geometries to represent other possible stack configurations including external reformation, co-flow, cross-flow and counter-flow manifolding.

System parameters that were calibrated for the bio-gas fed DFC system include the following:

- Active cell area and geometry (channel heights, lengths, and plate thicknesses)
- Fuel utilization (U_f)
- Ohmic and activation polarizations as a function of temperature
- Bio-gas composition
- Steam-to-carbon ratio (STC)
- Air inlet temperature and internal heating

The spatially resolved model output includes principal quantities such as local temperature and species concentrations in both anode and cathode, bulk channel flow rates, and resolved local current density. The balance of plant components include two water gas shift reactors, five heat exchangers, an oxidizer, two water condensers, an evaporator, an air blower, and six plenum volumes.

Measured data and literature results were used in place of detailed physical models for the air separation unit (ASU) and the PSA unit. The performance data used for the PSA unit was taken from direct communication with industrial partners. Similar performance parameters, a parasitic load of 7.812 kWh kg_{H2}^{-1}, was presented to the Association of Energy Engineers Southern California Chapter [21]. Air separation performance utilized values from the literature, 0.21 kWh kg_{O2}^{-1} [22]. The voltage characteristics of the MCFC were calibrated according to the fuel cell performance characteristics presented in Ref. [19] (Table 1).

This study, and the demonstration facility at Orange County Sanitation District, operate the MCFC under conditions different from those of the manufacturer performance sheet, namely higher fuel flow, lower air flow and higher cathode CO_2 concentration. The electrochemical impacts of higher anode hydrogen concentration and higher cathode CO_2 concentration are captured by the local calculation of Nernst potential and electrochemical losses. The thermal impacts of additional fuel reformation and reduced cathode heat transfer are captured by the spatially resolved energy balance in the fuel cell model.

The fuel reforming characteristics, specifically the ratio between indirect and direct internal reformation, play an important role in determining the performance of the MCFC. The exhaust composition is a combination of both processes and is what determines the CO_2 and H_2 available for capture. The exhaust values were calibrated with actual data from OCSD. Adjustments to the nominal MCFC operating conditions change the hydrogen recovery performance and the CO_2 sequestration potential through the exhaust composition as will be shown in the results section. The expressions and coefficients used to capture off-design MCFC performance including adjustments to overvoltage losses and reforming equations are reported in Appendix B.

4. CO_2 separation process

The objective of the current system integration is to recover carbon dioxide (and hydrogen) from the anode exhaust stream of the MCFC; typically comprised of CO, H_2O (steam), H_2 and CO_2. The water-gas shift and hydrogen separation occurring upstream of the CO_2 removal both serve to increase the CO_2 concentration of the

Table 1
List of parameters utilized in the fuel cell model.

P_{el} [kW]	300
Manifolds disposition	Cross-flow
Length [m]	1.1
Width [m]	0.8
Area [m^2]	0.88
Thickness of the cell (without gas channels) [m]	0.0025
Power density [mW cm^{-2}]	120
Number of cells	285
Steam-to-carbon ratio (molar)	2.5:1
Fuel utilization: U_f	0.65
Biogas composition (molar): y_{CH4}	0.65 CH_4 0.35 CO_2
Reformer typology	Indirect internal
Reformer position	Every 10 cells

anode effluent. Thus the HSU effectiveness directly impacts the recoverable CO_2. The components used to achieve a high purity of carbon dioxide are reported in Fig. 2.

The anode exhaust is first cooled to 350 °C prior to the first water gas shift reactor as the carbon monoxide conversion is favored at low temperatures. A second heat exchanger lowers the temperature to 200 °C prior to the low temperature water gas shift reactor. The combination of the two reactors achieves a high conversion of the CO balancing the faster kinetics occurring at 350 °C and the greater conversion efficiency that occur at 200 °C. A subsequent condenser removes most of the water. The gas entering the hydrogen separation unit contains H_2 at near 25% mole fraction.

The hydrogen separation process is an energy-intensive process, and the total amount recovered is directly proportional to the electric power consumption. The technology adopted at the existing OCSD plant is pressure swing adsorption (PSA). This process, common in large scale applications, recovers high purity H_2 (99.99%). The PSA functions on the principle that gases can be preferentially adsorbed and desorbed from certain surfaces at different pressures [25]. The system recovers approximately 70% of the available hydrogen. Higher recovery rates require significant compression work, exceeding the benefit of the additional hydrogen recovery, since hydrogen must be recirculated to maintain a minimum concentration at the PSA inlet. The PSA at the OCSD plant operates between 10 and 40 bar with an electric load of 58 kW, met by the nearly 300 kW electric output of the MCFC. Alternative techniques for hydrogen separation such as membrane separation and electrochemical separation could achieve similar integration with carbon recovery at higher net electrical efficiencies [26].

The off-gas stream (remaining constituents) exiting the PSA is comprised primarily of CO_2, H_2O, and H_2 with trace amounts of CO and CH_4. The most effective means of converting the remaining quantities of CH_4, CO and H_2 without introducing nitrogen is stoichiometric combustion with pure oxygen.

Air separation is a complex and energy-intensive process that could represent a substantial additional parasitic load on the MCFC output. However, the oxygen flow requirement for this particular use is small due to the small amount of hydrogen and carbon monoxide remaining in the gas mixture after the WGS and the HSU. At this scale it is most effective for the high purity oxygen to be purchased from an external producer. Significantly larger plants could consider on-site air separation. The current model includes the energy requirement of air separation (as if it was accomplished on-site), but not that of transportation and delivery, when calculating the system performance characteristics and efficiency. The production of high purity oxygen is assumed to require 0.21 kWh kg_{O2}^{-1} [22], which can be expressed also as 0.756 kW (g_{O2}^{-1}) s It is readily apparent that a higher recovery rate of hydrogen in the HSU reduces the required oxygen flow and thus the parasitic energy consumption in the ASU.

The final process of carbon recovery is the removal of water in a second condenser. The resulting carbon dioxide purity should exceed 96% by volume, depending upon the water removal capability of the second condenser. The total quantity of CO_2 recovered through this process is equal to the carbon present in the fuel minus the quantity vented to the atmosphere for configuration 1 and equal to the fuel plus the quantity of $CO_3^{=}$ ions that pass across the electrolyte for configurations 2 and 3 where the cathode carbon dioxide is supplied from the exhaust of an ICE. These configurations will be described in detail in the next section.

5. System description

This study will analyze three configurations for using MCFC to recover CO_2. These systems differ substantially in their net electrically efficiency and carbon recovery. The three systems are:

- Recirculation of the CO_2 from anode exhaust to cathode
- Separation and capture of internal combustion engine exhaust
- Enhanced CO_2 recovery with multiple MCFC stacks in series

5.1. Configuration 1: recirculation of the CO_2

In this case the only carbon source is the fuel supplied to the FC, and a portion of the anode exhaust is recirculated into the cathode to supply the necessary amount of carbon dioxide. This is similar to the design of existing commercial MCFC systems. Calculation of the CO_2 availability in the cathode is achieved using the Faraday's law expressed for this application in Equation (1).

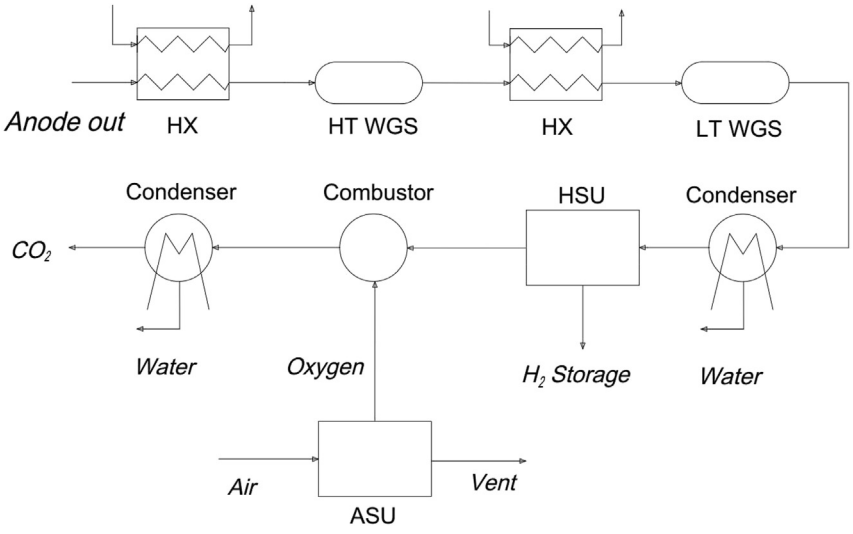

Fig. 2. CO_2 separation process.

$$\dot{N}_{CO_2,cath\ \ in} = \frac{I}{2F\ U_{CO_2}} \tag{1}$$

The current is directly measured, thus control of the carbon dioxide stream entering the cathode is possible with any arbitrary selection of a CO_2 utilization factor. Lower CO_2 utilization factors improve cell voltage marginally, however unutilized cathode CO_2 will escape into the environment with the cathode exhaust. Objectively, limiting the carbon dioxide concentration in the cathode exhaust will maximize the recoverable CO_2. Recovery of CO_2 from the cathode stream would require energy-intensive methods such as cryogenic separation or PSA.

The carbon recovery potential of different system configurations can be evaluated by establishing a CO_2 capture ratio (CCR). Equation (2) defines the CCR for this configuration as the maximum potential CO_2 recovery as a proportion of the fuel input of the MCFC. This expression assumes all carbon present in the anode outlet is converted to CO_2 and separated after two water gas shift reactors, an oxy-combustor, and a condenser. The quantity "1-CCR" embodies the flow of CO_2 released into the atmosphere. Due to inefficiencies and leakage in the HSU, and the condenser, real-world CCR will be only slightly reduced.

$$CCR = \frac{\dot{N}_{CO_{2_{capt}}}}{\dot{N}_{Carbon_{in}}} = \frac{\dot{N}_{Carbon_{Biogas\ to\ MCFC}} - \dot{N}_{CO_{2_{cat,in}}} \times (1 - U_{CO_2})}{\dot{N}_{Carbon_{Biogas\ to\ MCFC}}} = 1 - \frac{(1 - U_{CO_2})}{\frac{U_{CO_2}}{4U_f y_{CH_4}}} \tag{2}$$

The pinch analysis methodology was applied for determining the optimal heat integration among of the various heat demands/sources within the analyzed plant. The system does not require an external heat source and is capable of recovering thermal power at moderate and low temperatures from the cathode exhaust and the two condensers on the anode stream. The three sources of heat are the outlet streams from the anode (~620 °C), the cathode (~650 °C) and the oxidizer (~500 °C). The temperature difference between cathode and anode outlet is due to manifolds disposition (cross-flow) and cell geometry (rectangular). Those characteristics depend on the MCFC technology adopted by the producer [7]. Cathode flow rate is controlled with a blower in order to maintain a temperature difference of 100 °C between the inlet and the outlet of the cathode compartment. Cathode recirculation is another option for controlling air flow, but is not applied in the case of the DFC design. A detailed plant schematic for configurations 1 and 2 is presented in Fig. 3 (the values of each cornerstone are reported in the Appendix A). The dashed line represents the internal CO_2 recirculation of configuration 1. The pressure losses for an ambient pressure MCFC are responsible for the sizable cathode blower parasitic, but are not significant enough to affect the chemical kinetics, so they have been assumed constant in the current study. The baseline operating conditions for the MCFC tri-generation plant are specified in Table 2.

At a carbon dioxide utilization factor of 80%, Equation (2) determines a CCR of 56.4%. A carbon dioxide utilization factor of 80% implies a relatively low voltage which is undesirable. At U_{CO2} values higher than 90% (Fig. 4), the CO_2 starvation phenomenon takes place and concentration losses significantly affect the total voltage. In configurations 1 and 2 the maximum U_{CO2} value remains below this threshold, operating at an 80% utilization, in order to avoid issues of reactant starvation in the downstream regions of the

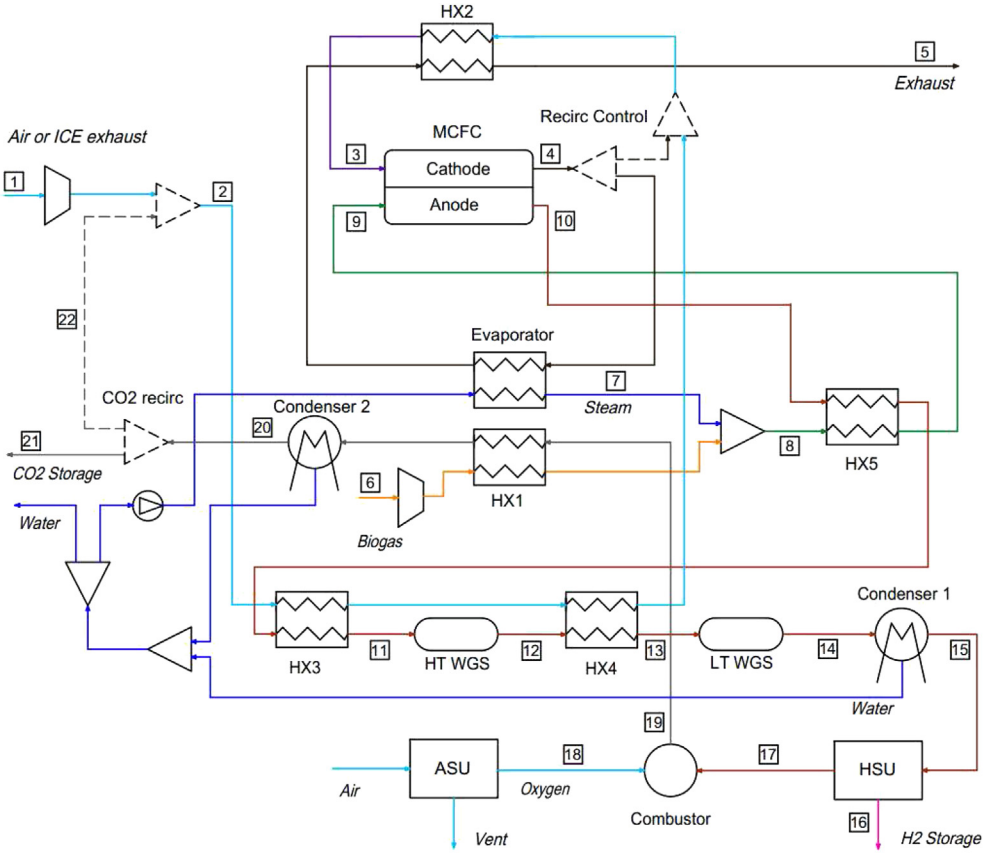

Fig. 3. System scheme (Configurations 1 and 2).

Table 2
Results (Configurations 1 and 2).

	Configuration 1	Configuration 2
Biogas composition (molar)	0.65 CH_4–0.35 CO_2	0.65 CH_4–0.35 CO_2
Flow rate Cathode/Biogas [kg s^{-1}]	2.124/0.035	1.912/0.033
Fuel Utilization, Uf (%)	65	65
CO_2 utilization (%) – UCO_2	80	32.4
Voltage [V]	0.677	0.733
Current [mA cm^{-2}]	177.5	163.1
Plant Electric Efficiency – η	0.322	0.362
η with hydrogen (LHV)	0.609	0.648
H_2 produced [g s^{-1}]	1.709	1.564
P_{el} stack [kW]	300	300
P_{el} plant [kW]	229.4	236.9
CO2 captured, vented [g s^{-1}]	33.67–25.17	147.42–194.49
Captured CO_2 purity (vol.)	0.978	0.978
CCR [%]	56.4	42.9
Cathode inlet [CO_2]/[O_2]	0.037/0.202	0.107/0.077
$T_{cathode}$ [°C] Inlet/Outlet	550/650	550/650
$T_{anode,}$ [°C] Inlet/Outlet	530/612	530/622
$P_{el,\ ICE}$ [kW]	–	1426

MCFC. This represents a practical operating condition for the MCFC which avoids the precipitous voltage drop at higher CO_2 utilizations. Note that examinations at very low reactant concentrations are only observable with a spatially discretized model, such as the one used in this study, where flow geometry partially mitigates the sudden onset of diffusion loses at high CO_2 utilizations.

Besides the electrochemical losses in the fuel cell, one must also consider the electric power consumed by the air blower and PSA compressors. Considering both the net electricity output and the chemical potential of the recovered hydrogen the co-production efficiency rises to 60.9% of the lower heating value of the biogas fuel. The recovered CO_2 purity is high (0.978) when the second water condenser effectiveness is similarly high.

5.2. Sensitivity analysis – Configuration 1

Fig. 5 shows the effects of fuel utilization variation, which can be manipulated by adjusting either fuel flow or current, or some combination thereof. Variation of U_f illustrates the direct dependence of CO_2 removal on H_2 separation. Increasing fuel utilization reduces the hydrogen recovery, and subsequently CO_2 recovery.

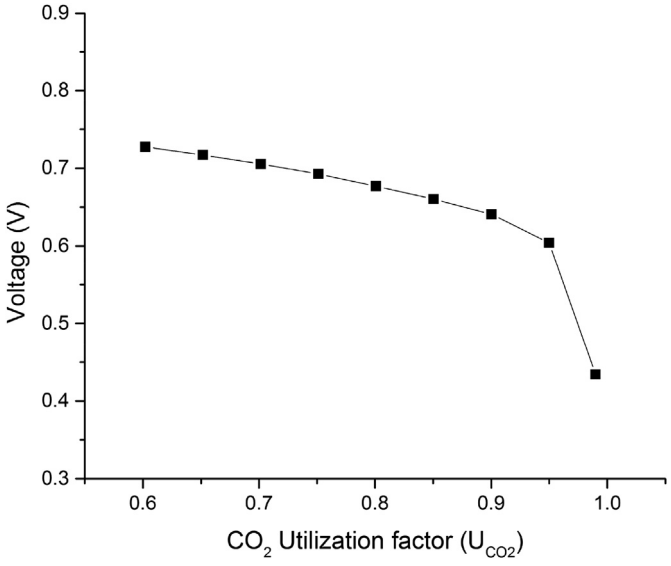

Fig. 4. U_{CO2} – Voltage.

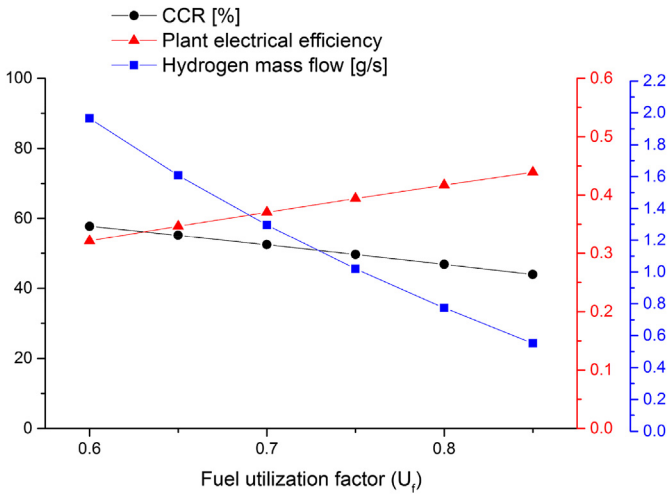

Fig. 5. Configuration 1, U_f variation.

Voltage drops, while net electrical efficiency rises. This relative low value is caused mainly by the HSU electrical consumption. Cathode air flow increases in proportion to the reduced voltage in order to maintain a constant internal temperature and temperature gradient. The additional cathode flow allows more CO_2 to escape unless the cathode CO_2 concentration is simultaneously reduced.

Fig. 6 highlights methane composition in the biogas, which is known to fluctuate substantially. Simple fuel control methods using voltage and current measurements can ensure the anode chemical potential remains nearly constant without sampling the fuel composition. The concentration of diluents in the biogas, chiefly CO_2, can reduce system voltage while increasing CCR potential. Fig. 5 illustrates how an increase in fuel CO_2 concentration (and thus a diminution of CH_4 concentration) increases CCR for the first configuration. This is understood since the bio-gas CO_2 remains entrained in the anode stream.

Fig. 7 illustrates the dependence of CCR on U_{CO2} (as demonstrated in the Equation (2)). The CO_2 utilization factor in the first configuration is a function of the anode exhaust injection into the cathode stream. Any excess CO_2 injection escapes with the cathode exhaust. Fig. 6 also shows the linear relationship between CO_2 utilization and hydrogen recovery. The stack electrical efficiency

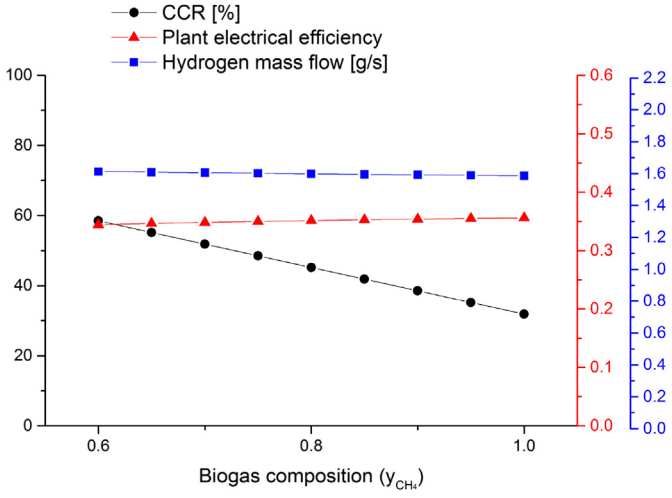

Fig. 6. Configuration 1, variation of methane composition in biogas.

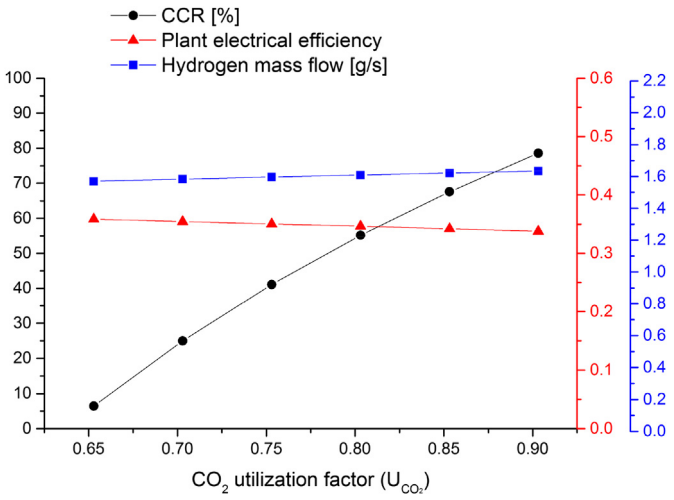

Fig. 7. Configuration 1, U_{CO2} variation.

slightly decreases as CO_2 utilization increases. Voltage and efficiency are affected by an increase in concentration overvoltage caused by limitations in CO_2 diffusion to the triple-phase-boundary. In particular, at high utilization the cathode CO_2 is close to stoichiometric and may be completely depleted in some cathode channels unless there is perfect manifolding and distribution of the oxidant stream. With stack power held constant at 300 kW, the current increases proportional to any voltage reduction. Oxygen utilization decreases with the rising U_{CO2} value, due to the additional air flow requirement for cooling. Lower electrochemical efficiency implies additional internal heat generation, and consequently rising air flow or rising temperature.

5.3. Configuration 2: internal combustion engine exhaust

The second configuration developed applies the exhaust of a separate ICE as the cathode oxidant feedstock. This integration removes the requirements for an air blower and for anode exhaust injection into the cathode stream. Without a means for controlling the cathode inlet concentration of CO_2 it is not possible to control the U_{CO2} as in the first configuration. Without anode exhaust injection the ICE must be of sufficient size to meet the O_2 and CO_2 requirement of the MCFC electrochemistry. This corresponds to an ICE: MCFC size ratio of 1.9:1 under nominal operating conditions. The ratio of ICE to MCFC electrical output will change as the O_2 and CO_2 requirements change with MCFC operating conditions. The ICE exhaust serves the additional purpose of providing the stack cooling flow. A 40% efficient ICE, operating on natural gas, with an exhaust flow matching the cathode flow requirement of an MCFC will contain 250% of the necessary CO_2, more for bio-gas and nearly 400% of the necessary O_2 for the electrochemical reactions. This corresponds to an ICE: MCFC size ratio of 4.66:1. Where the CO_2 exhaust of the ICE determines the smallest ICE size without anode exhaust injection, the cooling flow requirement determines the largest ICE size for which all of the ICE exhaust can be supplied to the MCFC. Between these two sizes some form of cathode recirculation or series connection of MCFC must be employed with intercooling to provide sufficient stack cooling. The ratio of MCFC to ICE size will influence the net cost, efficiency, CO_2 recovery and operational flexibility. This analysis will focus on the efficiency and CO_2 capture.

Cathode recirculation could partially decouple the inlet composition from flow rate, but without an additional source of CO_2 it will only serve to dilute both the inlet oxygen and CO_2 concentrations. Thus, a practical limit of cathode recirculation when using ICE exhaust is 20%. The ability to recirculate cathode exhaust is necessary if the ICE is to operate in a load following manner. All other system components are the same as for the previous reference configuration. A standard plant could readily be switched between self-CO_2 injection and this externally sourced CO_2 injection method, since the configuration of heat exchangers is very similar.

The ICE exhaust composition is calculated starting from the same biogas concentrations specified for the fuel cell. The electric power supplied by the biogas driven ICE is specified by $P_{el,ICE}$ and Equation (3). Since we are dealing most likely with large diesel ICE an engine efficiency of 40% is specified with the methane molar flow described by Equation (4) and Equation (5).

$$P_{el,\ ICE} = LHV_{CH_4} \times \dot{N}_{CH_4,biogas} \times \eta_{ICE} \tag{3}$$

$$\dot{N}_{CH_4,biogas} = \dot{N}_{CO_2,exhaust} \times y_{CH_4} \tag{4}$$

$$\dot{N}_{CO_2,\ exhaust} = \dot{N}_{exhaust} \times [CO_2] \tag{5}$$

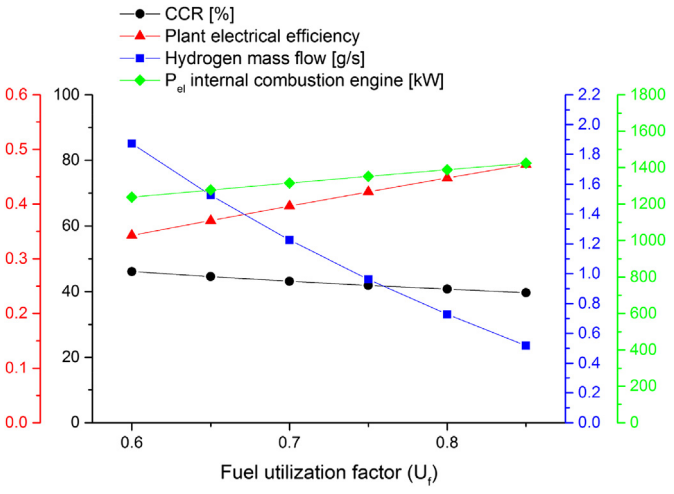

Fig. 8. Configuration 2, U_f variation.

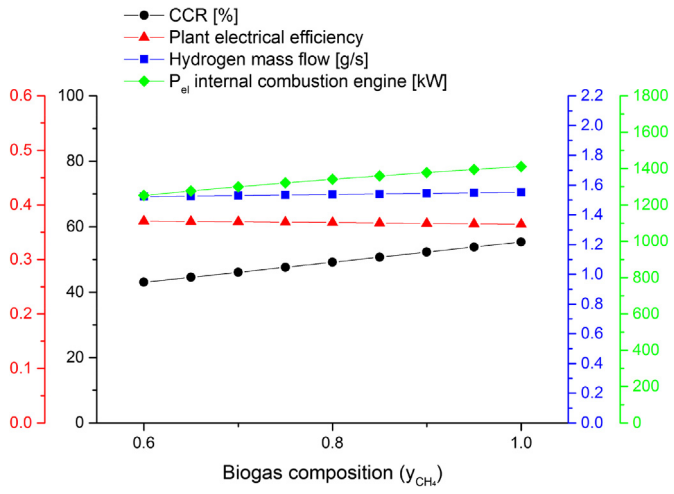

Fig. 9. Configuration 2, variation of methane composition in biogas.

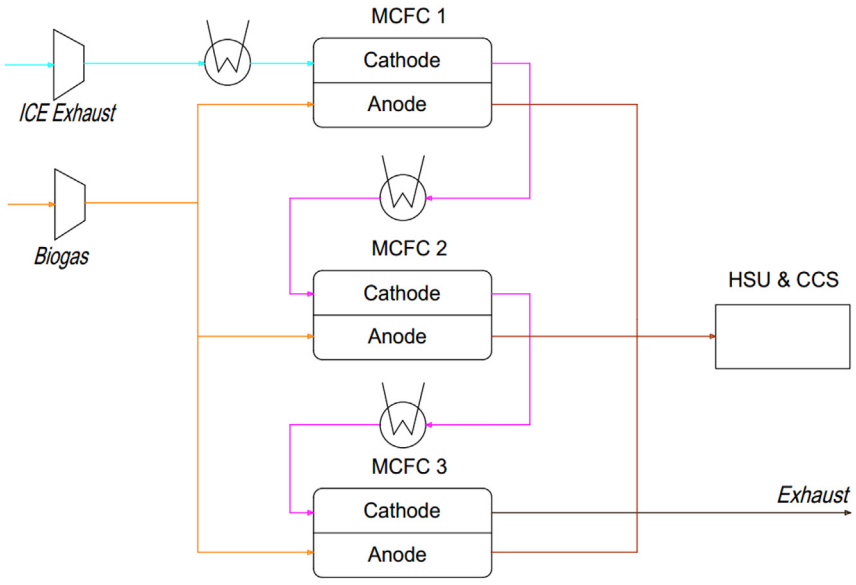

Fig. 10. Configuration 3, multiple stacks in series.

The ICE exhaust molar flow that feeds the cathode is calculated by the model in order to maintain the temperature difference of 100 K between inlet and outlet, while the carbon dioxide concentrate on depends upon the biogas concentration and upon the air index.

The efficiency and exhaust composition define the ICE system output, which can be successfully integrated with the MCFC CO_2 recovery system. The CCR for this configuration (Equation (6)) is calculated as the ratio of the carbon recovered to the carbon that enters in the system in the form of biogas fuel to both the ICE and MCFC. Fig. 3 also illustrates this second configuration when internal recirculation of CO_2 is replaced with ICE exhaust.

$$CCR = \frac{\dot{N}_{CO_{2_{capt}}}}{\dot{N}_{BIOGAS_{an.in}} + \dot{N}_{BIOGAS_{ICE}}} \tag{6}$$

Since none of the CO_2 participating in the electrochemistry is subsequently injected into the cathode and exhausted, as for the configuration 1, simulations indicate a fourfold increase in the amount of CO_2 recovered despite the lower CCR value of 42.95% (Table 2). At this largest size ratio, 1.4 MW ICE paired with a 300 kW MCFC, there is substantial excess CO_2 available resulting in a lower U_{CO2} and a potential co-benefit of higher cell voltage due.

5.4. Sensitivity analysis – Configuration 2

As in the previous configuration, Fig. 8 shows that fuel utilization within the MCFC can be readily controlled. The impact on CCR exhibits similar trends, albeit with less variation. The equivalent electric power increases with U_f, due to the reduced parasitic of the HSU. The HSU parasitic is reduced because there is less hydrogen available to recover. Electric performance remains strongly dependent upon U_f. The results indicate a co-production flexibility, as it is possible to alter the ratio of hydrogen and electric production without dramatically impacting CCR.

The impact of varying biogas fuel composition was also investigated for this configuration (Fig. 9). The primary difference is that the same biogas now feeds both the MCFC and the ICE. Hydrogen recovery and plant electrical efficiency do not change with the biogas variation, while CCR increases slightly. In particular, an increase in methane concentration lowers the ICE exhaust CO_2 concentration and subsequently increases U_{CO2}. Moreover, feeding the plant with pure methane ($y_{CH4} = 1$) involves the utilization of an engine with a nominal electric power that is increased compared to the standard case ($y_{CH4} = 0.65$).

5.5. Configuration 3: multiple stacks in series

A smaller ratio of ICE to MCFC sizes can result in much higher CO_2 recovery, but requires some form of cathode recirculation and intercooling to achieve sufficient stack cooling. This configuration will consider the same 1.4 MW ICE paired with multiple 300 kW MCFC systems connected in series with cathode exhaust heat recovery placed between them as illustrated in the Fig. 10.

The internal combustion engine feeds the first MCFC cathode which subsequently supplies the second and third MCFC. Each MCFC requires a similar quantity of biogas. Thus, the total biogas flow to the fuel cell is tripled. The electric output and hydrogen

Table 3
Results (Configuration 3).

Cross-flow configuration								
	P_{el} [kW]	CCR_{TOT}	CCR_{STACK}	U_{CO2}	ΔT_{cath} [K]	η_{STACK}	$H_{2,\ STACK}$ [g/s]	$H_{2,\ TOT}$ [g/s]
1° MCFC	300	0.419	0.419	0.316	100	0.454	1.586	1.586
2° MCFC	300	0.734	0.5248	0.414	101	0.438	1.604	3.19
3° MCFC-A	300	0.984	0.773	0.689	112	0.414	1.737	4.927
3° MCFC-B	150	0.868	0.755	0.664	110	0.415	0.874	4.064

recovery are similarly tripled. This solution does not add to the HSU or carbon recovery balance of plant as the separate anode streams can be readily combined into a single effluent and handled as in configurations 1 and 2. The first two cathode outlet flow streams are cooled before entering downstream cathode compartments.

The two obstacles of this solution are: 1) With additional MCFC in series the U_{CO2} of the downstream systems increases considerably and these may experience the performance loss as described in the first configuration, and 2) Independent control of the temperature gradient is complicated by the coupling of the cathode flow rates. This problem could be limited by adding an additional air flow stream, but this solution would further dilute the CO_2 concentration.

For these reasons, a practical limit to this series configuration was selected as 3 systems in series. Additional series and parallel configurations are potentially possible depending upon the electrical power requirements and biogas availability.

The CCR for this series connected configuration is calculated using Equation (7)

$$CCR = \frac{\sum \dot{N}_{CO_{2_{capt}}}}{\dot{N}_{Biogas\,to\,1^{\circ}\,MCFC} + \dot{N}_{Biogas\,to\,2^{\circ}\,MCFC} + \dot{N}_{Biogas\,to\,3^{\circ}\,MCFC} + \dot{N}_{ICE}} \quad (7)$$

Table 3 summarizes the primary performance characteristics of the series connected configuration. The first row, 1st MCFC, represents the original configuration while the 2nd and third rows represent two and three systems connected in series. The High U_{CO2} in the third fuel cell resulted in significant performance loss, thus a final configuration of 2.5 systems in series was considered and presented in the last row of Table 3.

The two issues described previously, the progressive increase of U_{CO2} and cathode ΔT, are apparent in the increased heat generation of the downstream MCFC. The temperature gradient is constrained by materials constraints, and thus exceeding this limit can be dangerous for the life of the stack. The third MCFC would be expected to be the most likely to exceed temperature limits due to the increased U_{CO2} and fixed cathode flow. This can be solved by operating downstream MCFC at reduced power to maintain the same voltage as the upstream systems. The CCR in a series connected system exceeds 73% for two systems in series and exceeds 90% for 3 systems in series, when operated in this manner. This remarkably high carbon recovery is possible with the majority of the power still delivered by the low cost ICE system, 1.4 MW of 2.3 MW total. The system retains its hydrogen co-production capability and offers additional opportunity for high quality waste heat recovery between the high temperature fuel cells.

6. Summary and conclusions

Three possible configurations were outlined and studied; a standalone MCFC tri-generation plant, the same plant integrated with exhaust from an ICE plant, and the ICE-MCFC hybrid integrated with additional MCFC plants in a series configuration. The systems described could be readily deployed using existing commercial systems. Moreover, the first and the second configurations, while appearing more complex, could be realized in a single system with some valve design and controls for switching between ICE exhaust and CO_2 injection from anode recirculation. A series configuration of MCFC technology coupled with an ICE achieves outstanding carbon recovery (exceeding 90%), with minimal parasitic load; that of the production of O_2 in an ASU and the cooling fan in the second condenser.

Carbon separation and hydrogen co-production processes are compatible and benefit from the carbonate ion charge carrying properties of a molten carbonate fuel cell. Hydrogen co-production reduces fuel-to-electric efficiency due to the PSA parasitic load and lower operating fuel utilization used to generate excess hydrogen. All three configurations achieved notable carbon removal with minimal parasitic load. Configuration 1 (standalone system) required a high CO_2 utilization factor (>75%) in order to separate a sufficient carbon quantity. Possible drawbacks to carbon recovery from a MCFC tri-generation system include complex thermal integration due to additional heat exchange steps as well as reduced fuel-to-electric efficiency due to the low fuel utilization and high parasitic electric load of the HSU and any additional compression of CO_2 and H_2 products not considered in this analysis.

Appendix A: cornerstones for the configurations 1 and 2

Table 4
Cornerstones (Configuration 1).

	T [°C]	X_{CH_4}	$\mathbf{X}_{CO}$	X_{CO_2}	X_{H_2}	X_{H_2O}	X_{N_2}	X_{O_2}	$\dot{N}$ [Mol s^{-1}]	$\dot{m}$ [kg s^{-1}]
1	27						0.790	0.210	73.655	2.124
2	26			0.038		0.001	0.760	0.202	76.602	2.252
3	550			0.038		0.001	0.760	0.202	76.602	2.252
4	651			0.008		0.001	0.796	0.196	73.141	2.114
5	159			0.008		0.001	0.796	0.196	73.141	2.114
6	27	0.650		0.350					1.365	0.035
7	234					1			2.219	0.040
8	387	0.248		0.133		0.619			3.584	0.075
9	530	0.248		0.133		0.619			3.584	0.075
10	612		0.050	0.429	0.112	0.409			7.667	0.214
11	350		0.050	0.429	0.112	0.409			7.667	0.214
12	361		0.011	0.468	0.151	0.370			7.667	0.214
13	199		0.011	0.468	0.151	0.370			7.667	0.214
14	206		0.003	0.476	0.159	0.362			7.667	0.214
15	10		0.005	0.728	0.244	0.024			5.012	0.166
16	10				1				0.854	0.002
17	10		0.005	0.878	0.088	0.028			4.157	0.164
18	10							1	0.194	0.006
19	526			0.881	0.002	0.115		0.001	4.141	0.169
20	10			0.979	0.002	0.017		0.001	3.729	0.162
21	30			0.979	0.002	0.017		0.001	0.782	0.034
22	30			0.979	0.002	0.017		0.001	2.947	0.128

Table 5
Cornerstones (Configuration 2).

	T [°C]	X_{CH_4}	$\mathbf{X}_{CO}$	X_{CO_2}	X_{H_2}	X_{H_2O}	X_{N_2}	X_{O_2}	$\dot{N}$ [Mol s^{-1}]	$\dot{m}$ [kg s^{-1}]
1	24			0.108			0.815	0.077	63.690	1.913
2										
3	550			0.108			0.815	0.077	63.690	1.913
4	650			0.078			0.859	0.063	60.477	1.784
5	114			0.078			0.859	0.063	60.477	1.784
6	27	0.650		0.350					1.267	0.033
7	292					1			2.060	0.037
8	413	0.248		0.133		0.619			3.327	0.070
9	530	0.248		0.133		0.619			3.327	0.070
10	607		0.049	0.430	0.113	0.408			7.117	0.198
11	350		0.049	0.430	0.113	0.408			7.117	0.198
12	361		0.011	0.468	0.151	0.370			7.117	0.198
13	200		0.011	0.468	0.151	0.370			7.117	0.198
14	207		0.003	0.476	0.159	0.362			7.117	0.198
15	10		0.004	0.728	0.244	0.024			4.654	0.154
16	10				1				0.794	0.002
17	10		0.005	0.878	0.088	0.028			3.859	0.152
18	10							1	0.180	0.006
19	524			0.881	0.002	0.115		0.001	3.846	0.157
20										
21	10			0.979	0.002	0.017		0.001	3.463	0.150
22										

Appendix B: overvoltage and reforming equations

Nernst potential and overvoltage losses

The Nernst potential is related to the Gibbs energy by the Faraday's law and the number of electrons consumed in the reduction reaction (Equation (B1)). Nearnst potential is calculated locally using local bulk flow species concentrations and temperatures.

$$E = \frac{\Delta G^0}{2F} - \frac{R\,T}{2\,F}\ln\left(\frac{p_{an_{H_2}} p_{cat_{CO_2}} p_{cat_{O_2}}^{0.5}}{p_{an_{CO_2}} p_{an_{H_2O}}}\right) \tag{B1}$$

In order to obtain the local voltage of the cell, it is necessary to subtract the three overvoltage losses (e.g. η_{act}, η_{ohm}, η_{conc}) from the Nernst potential. The expressions utilized to calculate the activation, ohmic, and concentration loses are detailed in Equations (B2)–(B4). An equipotential constraint is used to solve for the spatial current distribution which balances the temperatures and concentration variation. The activation overvoltage, η_{act}, is related to the charge transfer from the molecule to the electrode (oxidation) and vice versa (reduction). Equation (B2) relates the activation polarization and the current density through the Tafel's law, where "i_0" is the exchange current density (300 A m^{-}2) and á is the charge transfer coefficient (0.4).

$$\eta_{act} = \frac{\mathrm{R}\,T}{\alpha\, n\,\mathrm{F}}\ln\left(\frac{i}{i_0}\right) \tag{B2}$$

The ohmic overvoltage, η_{ohm}, is significant due to the poor electrical conduction of the electrodes. The conduction is highly temperature dependent. This model utilized an empirical expression for the resistance proposed by Rivera [23].

$$\eta_{ohm} = i\cdot[(4.7833\ \mathrm{e}-04) - (\,6.6667\ \mathrm{e}-07)(T-273)] \tag{B3}$$

The concentration overvoltage, η_{conc}, is associated with diffusion of bulk reactant flows to the triple phase boundary. The diffusion loses are modeled with a logarithmic function with an empirically identified current density limit, i_L (6000 A m^{-2}).

$$\eta_{conc} = \left(1+\frac{1}{\alpha}\right)\frac{R\,T}{n\,F}\ln\left(\frac{i_L - i}{i_L}\right) \tag{B4}$$

Fuel reformation and species consumption

Local species and temperatures were determined with the application of appropriate chemical kinetics, heat transfer and conservation equations within the reformer and anode channels. The overall consumption (or accumulation) of species in the bulk flow is determined with Equation (B5). The terms, $\dot{N}_i$, X_i, $\boldsymbol{R}_i$, P, and V represent respectively: the molar flow rate, bulk flow concentration, net molar production of reforming or electrochemical reactions, the local pressure, and the control volume of the anode/reformer channels. The rate of species consumption by the electrochemical reactions, $\boldsymbol{R}_{CONSUME}$, is determined using Faraday's law and the current determined to balance the voltage and power expressions.

$$\frac{dX_{i,out}}{dt} = \frac{\boldsymbol{R}_{REFORM} + \boldsymbol{R}_{WGS} + \boldsymbol{R}_{CONSUME} + \dot{N}_{in}X_{i,in} - \dot{N}_{out}X_{i,out}}{\frac{P_j V_j}{R_u T_j}} \tag{B5}$$

The rate of species conversion within the reformer and anode channels, $\boldsymbol{R}_{REFORM} + \boldsymbol{R}_{WGS}$, is determined from the chemical kinetics of steam methane reformation and water gas shift reactions. Other chemical reactions can take place, but they occur at a much slower rate which allows a model to maintain accuracy when neglecting them. The methane reforming rate uses an empirical correlation (Equation (B6)) developed by Seo et al. [24]. The water gas shift reaction (Equation (B7)) has been adopted from Haberman and Young [23], and was developed specifically for the high temperature conditions of a fuel cell anode.

$$R_{REFORM} = A_{cell}\cdot p_{CH_4}\exp\left[-\frac{8.2\times 10^4}{R_u T}\cdot 2137\times 10^6\right] \tag{B6}$$

$$R_{WGS} = A_{cell} \cdot p_{CO}\, 0.0171 \exp\left[-\frac{103191}{R_u T}\right] \times \left(1 - \frac{p_{CO_2}\, p_{H_2}}{\exp\left[\frac{4276}{T} - 3.1961\right] p_{CO}\, p_{H_2O}}\right) \quad \text{(B7)}$$

References

[1] Intergovernmental Panel on Climate Change, Climate Change 2013: the Physical Science Basis, Cambridge University Press, 2013.
[2] United Nations Framework Convention on Climate Change. Kyoto Protocol. http://unfccc.int/resource/docs/publications/08_unfccc_kp_ref_manual.pdf.
[3] U.S. Energy Information Agency, DOE Energy Information Agency Annual Energy Outlook, 2013. http://www.eia.gov/forecasts/aeo/pdf/0383(2013).pdf.
[4] L.I. Mu, A.D. Rao, J. Brouwer, G. Scott Samuelsen, Design of highly efficient coal-based integrated gasification fuel cell power plants, J. Power Sources 195 (2010) 5707–5718.
[5] G. Göttlicher, R. Pruschek, Comparison of CO_2 removal systems for fossil-fuelled power plant processes, Energy Convers. Manag. 38 (1997) S173–S178.
[6] A. Lanzini, T.G. Kreutz, E. Martelli, M. Santarelli, Energy and economic performance of novel integrated gasifier fuel cell (IGFC) cycles with carbon capture, Int. J. Greenh. Gas Control 26 (2014) 169–184.
[7] FuelCell Energy. www.fuelcellenergy.com.
[8] Bloom Energy. http://www.bloomenergy.com.
[9] P. Margalef, T. Brown, J. Brouwer, S. Samuelsen, Conceptual design and configuration performance analyses of polygenerating high temperature fuel cells, J. Hydrog. Energy 36 (2011) 10044–10056.
[10] California Environmental Protection Agency, California's Hydrogen Transportation Initiatives, 2014. http://www.arb.ca.gov/msprog/zevprog/hydrogen/hydrogen.htm.
[11] X. Li, J. Ogden, C. Yang, Analysis of the design and economics of molten carbonate fuel cell tri-generation systems providing heat and power for commercial buildings and H_2 for FC vehicles, J. Power Sources 241 (2013) 668–679.
[12] Fuel cell today document. http://www.fuelcelltoday.com/media/1637141/using_fc_converting_waste_to_energy.pdf.
[13] K. Sugiura, K. Takei, K. Tanimoto, Y. Miyazaki, The carbon dioxide concentrator by using MCFC, J. Power Sources 118 (2003) 218–227.
[14] S. Campanari, P. Chiesa, G. Manzolini, CO_2 capture from combined cycles integrated with molten carbonate fuel cells, J. Greenh. Gas Control 4 (2010) 441–445.
[15] P. Chiesa, S. Campanari, G. Manzolini, CO_2 cryogenic separation from combined cycles integrated with molten carbonate fuel cells, J. Hydrog. Energy 36 (2011) 10355–10365.
[16] D. Sànchez, B. Monje, R. Chacartegui, S. Campanari, Potential of molten carbonate fuel cells to enhance the performance of CHP plants in sewage treatment facilities, J. Hydrog. Energy 38 (2013) 394–405.
[17] U. Desideri, S. Proietti, P. Sdringola, G. Cinti, F. Curbis, MCFC-based CO_2 capture system for small scale CHP plants, J. Hydrog. Energy 37 (2012) 19295–19303.
[18] D. McLarty. PhD. thesis, University of California, Irvine. 2010.
[19] D. McLarty, A spatially resolved physical model for transient system analysis of high temperature fuel cell, J. Hydrog. Energy 38 (2013) 7935–7946.
[20] J. Brouwer, F. Jabbari, E. Leal, T. Orr, Analysis of a molten carbonate fuel cell: numerical modeling and experimental validation, J. Power Sources 158 (2006) 213–224.
[21] J. Brouwer, High Temperature Fuel Cell Tri-generation of Power, Heat & H2 from Waste, 2012. https://www.aeesocal.org/docs/chapterMeeting/48-tri-generation_ocsd_overview_aee_120612xs.pdf.
[22] Chao Fu, T. Gundersen, Using exergy analysis to reduce power consumption in air separation units for oxy-combustion processes, Energy 44 (2012) 60–68.
[23] B. Haberman, J. Young, Three-dimensional simulation of chemically reacting gases in the porous support structure of an integrated-planar solid oxide fuel cell, J. Heat Mass Transf. 47 (2004) 3617–3629.
[24] Yong-Seog Seo, Dong-Joo Seo, Yu-Taek Seo, Wang-Lai Yoon, Investigation of the characteristics of a compact steam reformer integrated with a water-gas shift reactor, J. Power Sources 161 (2006) 1208–1216.
[25] S. Sircar, T.C. Golden, Purification of hydrogen by pressure swing adsorption, Sep. Sci. Technol. 35 (2000) 667.
[26] W.L. Becker, R.J. Braun, M. Penev, M. Melainab, Design and technoeconomic performance analysis of a 1 MW solid oxide fuel cell polygeneration system for combined production of heat, hydrogen, and power, J. Power Sources 200 (2012) 34–44.